Supplementary Information (SI) for Journal of Materials Chemistry A.
This journal is © The Royal Society of Chemistry 2026

Electronic Supplementary Information

Experimental section

Materials

Uranyl nitrate hexahydrate ($UO_2(NO_3)_2 \cdot 6H_2O$), sodium sulfate (Na_2SO_4), nitric acid (HNO_3), sulfuric acid (H_2SO_4), sodium hydroxide (NaOH), iron chloride ($FeCl_3$), potassium ferrocyanide trihydrate ($K_4Fe[CN]_6 \cdot 3H_2O$), arsenazo III were analytical reagents purchased from Aladdin Biochemical Technology Co., Ltd. Tannic acid ($C_{76}H_{52}O_{46}$, TA), phytic acid ($C_6H_{18}O_{24}P_6$, PA), phosphate buffered saline solution (PBS, 0.1 M), 3-(N-morpholino) propane sulfonic acid solution (MOPS, primary reagent) were obtained from the Macklin Biochemical Technology Co., Ltd. Ultrapure water produced by the Millipore DI system (Synergy 185, 18.2 MΩ cm) was used throughout all experiments. The carbon felt (CF, porosity = 51%, average pore size 162 μm, thickness = 2.0 mm) was obtained from CeTech Co., Ltd. and thoroughly washed by sonication in acetone, ethanol and water for 15 min, sequentially. The filtered real seawater was collected from the Bohai Sea near the east coast of Qingdao city, China.

Electrode preparation

All electrodes were fabricated on pre-cleaned carbon felt (CF, 1.0 × 1.5 cm^2) via a sequential coordination-driven self-assembly process. The core design features a robust Fe-TA network as an inner stabilizing layer, followed by an Fe-PA complex as the outer uranium-binding layer. A cleaned CF piece was immersed in 5 mL of aqueous TA solution (24 mM) for 10 min. Subsequently, 5 mL of $FeCl_3$ solution (24 mM) was added to form the initial Fe-TA coordination network upon gentle vortexing. The Fe-TA network on the CF substrate was stabilized by adding 10 mL of 100 mM MOPS (pH 7.4). After standing for 10 min, the piece was retrieved and thoroughly rinsed with deionized water and ethanol, yielding the intermediate product CF@MTN. The as-prepared CF@MTN was further functionalized by immersing it in 2 mL of PA solution (24 mM) for 10 min. Then, 6 mL of $FeCl_3$ solution (24 mM) was added to cross-link the PA, followed by a brief vortexing and a 10 min standing. Subsequently, 10 mL of 100 mM MOPS (pH 7.4) was added to complete the assembly of Fe-PA. After aging for 10 min and thorough washing, the final product was obtained and denoted as CF@MTPN. MOPS buffer was used to maintain a stable pH during

assembly, which is critical for controlled ligand deprotonation and uniform coating growth. The buffer was removed by extensive washing after coating.

For electrochemical measurements, the electrode (exposed area: 3.8 cm^2) was secured with a Pt clip. The average mass of the CF@MTPN electrode was 79.5 mg. For comparison, a control electrode without the inner Fe-TA layer was prepared. A bare CF piece was directly subjected to the same PA/$FeCl_3$ coating procedure described above for the second step of CF@MTPN synthesis. This sample, designated as CF@MPN, was used to elucidate the critical role of the Fe-TA inner layer in enhancing electrode stability.

Material characterization

Scanning electron microscopy (SEM) imaging was performed on a Gemini 300 field-emission microscope (Zeiss, Germany) operating at an accelerating voltage of 3 kV. Transmission electron microscopy (TEM) was conducted on a Talos F200S microscope (FEI, USA) at 200 kV. X-ray diffraction (XRD) data were collected using an X'Pert PRO MPD diffractometer (Rigaku Smartlab, Japan) with Cu Kα radiation. X-ray photoelectron spectroscopy (XPS) measurements were acquired on a Scientific K-Alpha spectrometer (Thermo Fisher, USA). Zeta potentials were determined with a Surpass Electrokinetic Analyzer (Anton Paar GmbH, Austria). Water contact angles were measured at ambient temperature (~30% humidity) by the sessile drop method using a JY-PHa instrument (China). UV-Vis absorption spectra were recorded on a UV-2700 spectrophotometer (SHIMADZU, Japan). Fourier transform infrared (FTIR) spectra were obtained using a Nicolet IS10 spectrophotometer (Thermo Fisher, USA). The concentration of uranium adsorbed onto the material surfaces was quantified by inductively coupled plasma mass spectrometry (Agilent 7900, USA). The pH values of all electrolytes were measured with a PHS-2F pH meter (Leici, China). Electrochemical measurements, including cyclic voltammetry (CV), linear sweep voltammetry (LSV), and electrochemical impedance spectroscopy (EIS), were performed on a CHI 760E electrochemical workstation (China) employing a standard three-electrode system.

Electrochemical measurements

All electrochemical measurements were performed using a CHI 760E electrochemical workstation under ambient conditions with a standard three-electrode configuration. The working electrodes were the as-prepared samples secured with Pt clips. A Pt wire

and a saturated calomel electrode (SCE, in saturated KCl) were employed as the counter and reference electrode, respectively. CV and LSV were conducted at scan rates of 5 mV s^{-1}, respectively, unless otherwise stated. EIS measurements were carried out in a 10 mM $K_3[Fe(CN)_6]/K_4[Fe(CN)_6]$ (1:1) solution over a frequency range from 100 kHz to 0.1 Hz. All potentials are reported versus the SCE unless specified.

Physicochemical adsorption experiment

The adsorption experiments were conducted at room temperature. Three pieces of the sample (1.0 × 1.0 cm^2 each) were added to 60 mL of uranyl solution (5 mg L^{-1}) under constant stirring. At predetermined time intervals, aliquots of the solution were withdrawn. The residual uranium concentration in these aliquots was analyzed by ICP-OES. The uranyl removal efficiency was calculated by the following equation:

$$Removal\ (\%) = \frac{C_0 - C_t}{C_0} \times 100\% \qquad (Eq.S1)$$

Where C_0 (mg L^{-1}) is the initial concentration of uranyl, and C_t (mg L^{-1}) is the concentration at time "*t*". All experiments were performed in triplicate, and the reported data are the average values.

Evaluation of uranium extraction performance

The uranium concentration in solution was quantified using two complementary techniques, selected based on the solution matrix. For solutions without carbonate interference, the concentration of residual UO_2^{2+} was determined by the arsenazo III colorimetric method.[1] For solutions containing carbonate, which interferes with the colorimetric assay, inductively coupled plasma optical emission spectrometry (ICP-OES) was employed.

The uranium extraction capacity of the CF@MTPN electrode was estimated by the following equation:

$$Extraction\ capacity = \frac{C_0 \times V_0 \times Removal \times 88.15\%}{m_0 \times 0.010417\ d^{-1}} \qquad (Eq.S2)$$

Where C_0 (mg L^{-1}) is the initial uranyl concentration, V_0 (L) is the solution volume, m_0 (g) is the mass of the dry CF@MTPN electrode, and *Removal* (%) is the average uranium removal rate at 15 min over 96 consecutive cycles without any regeneration. The value was converted to the mass of elemental uranium by applying the mass fraction of uranium in the uranyl ion (88.15%).

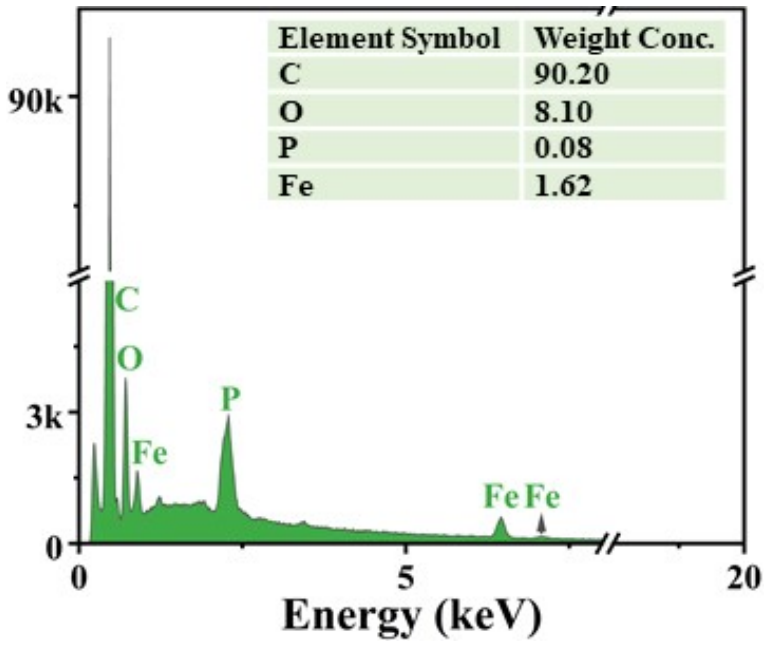

Fig. S1. EDX spectrum of CF@MTPN.

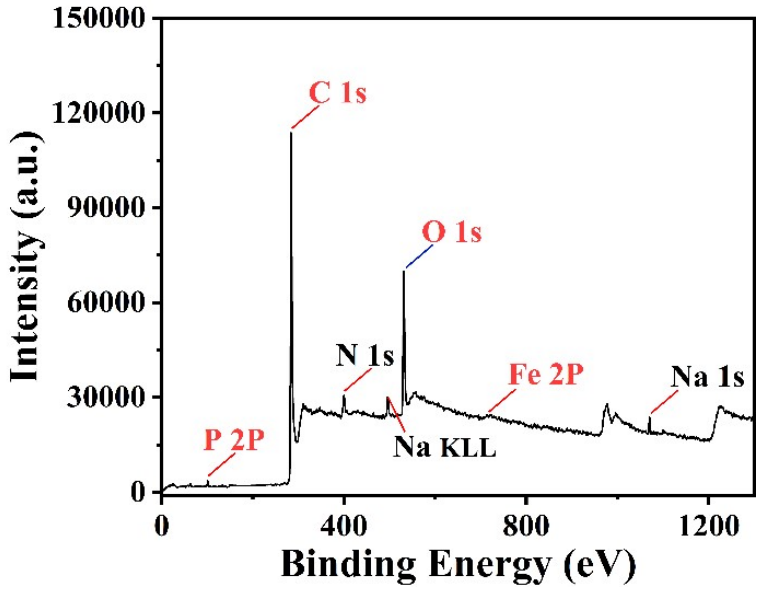

Fig. S2. XPS survey spectrum of CF@MTPN.

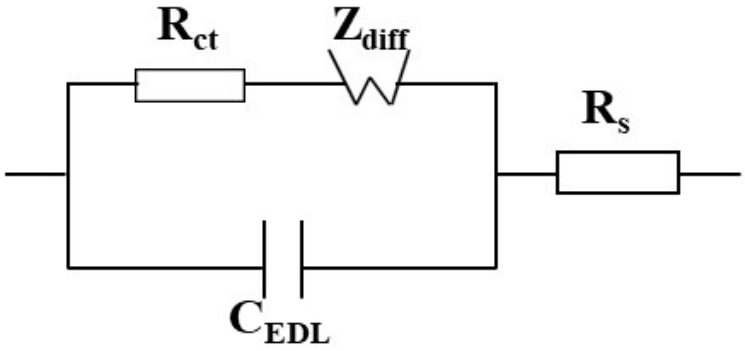

Fig. S3. The typically Randles–Ershler equivalent circuit with an EDL capacitance in one branch and a faradaic impedance in the other.

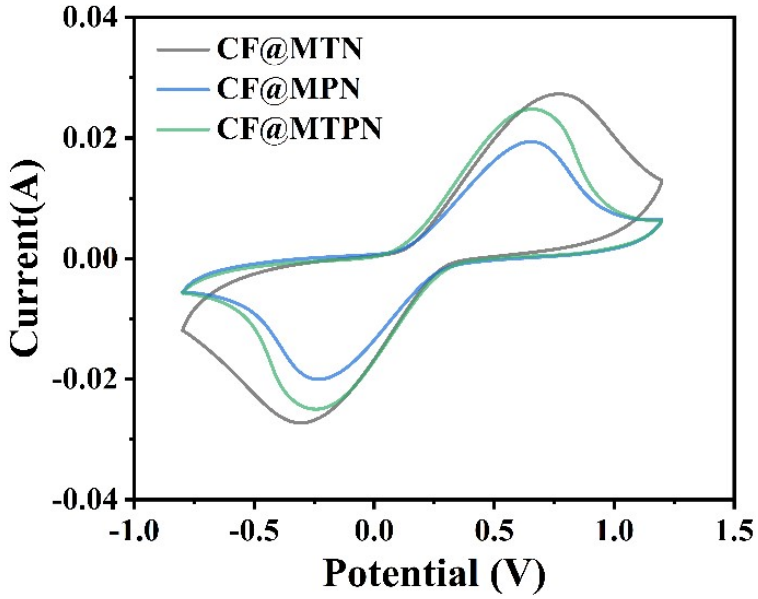

Fig. S4. CV curves of CF@MTN, CF@MPN and CF@MTPN in the solutions containing 0.1 M KCl, 5.0 mM $K_3[Fe(CN)_6]$ and 5.0 mM $K_4[Fe(CN)_6]$.

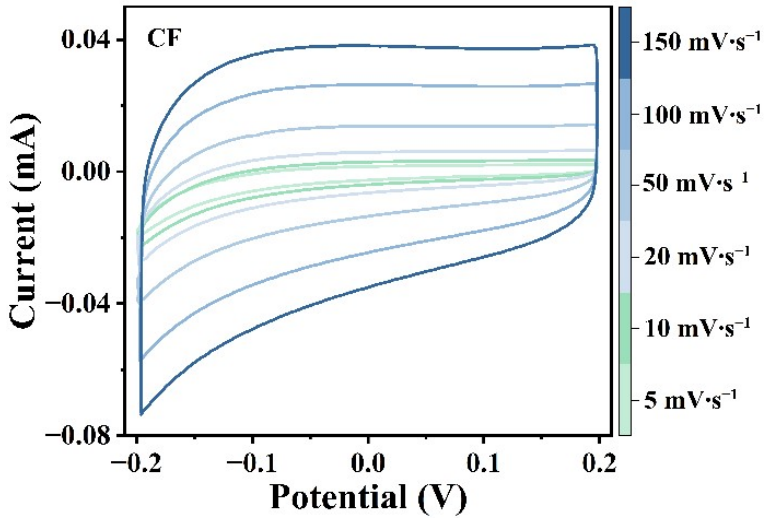

Fig. S5. CV curves of CF in 0.1 M Na_2SO_4 solution at different scan rates.

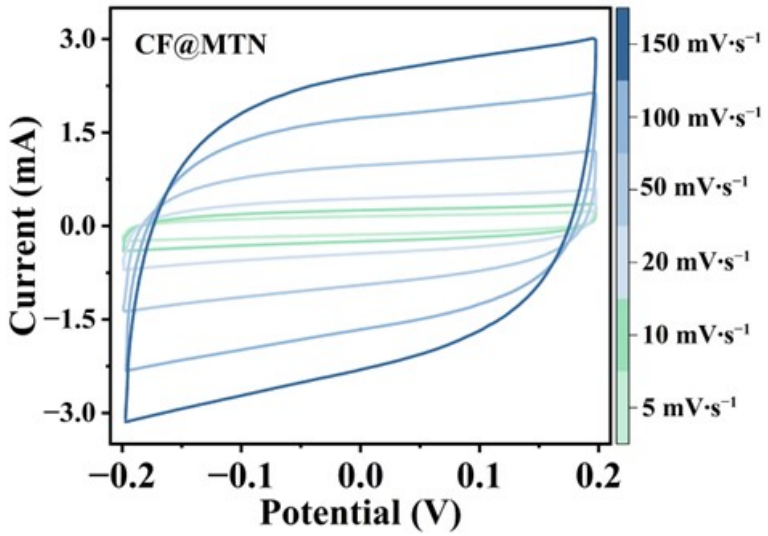

Fig. S6. CV curves of CF@MTN in 0.1 M Na_2SO_4 solution at different scan rates.

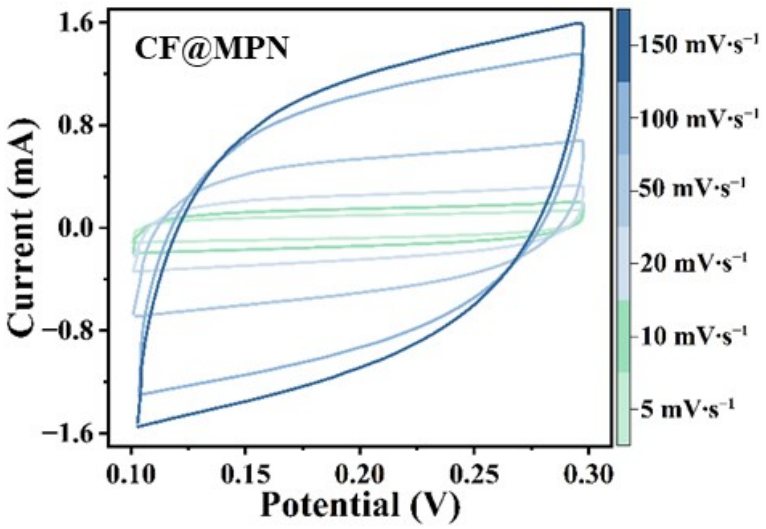

Fig. S7. CV curves of CF@MPN in 0.1 M Na_2SO_4 solution at different scan rates.

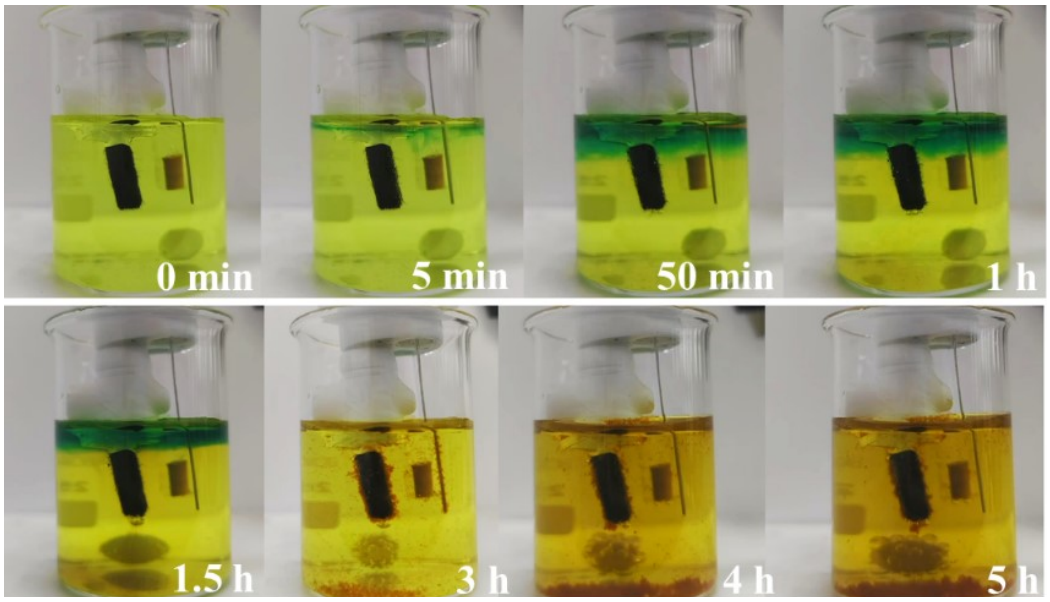

Fig. S8. Photographs of the precipitation formation by CF@MTPN.

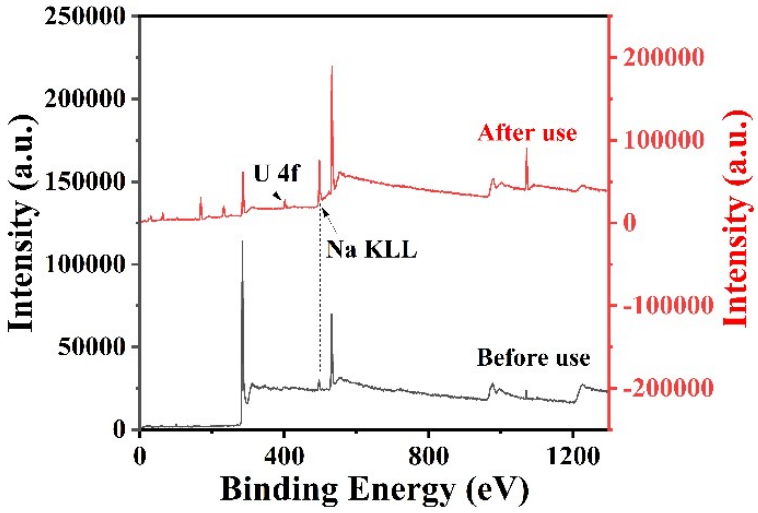

Fig. S9. XPS survey maps of CF@MTPN before and after use.

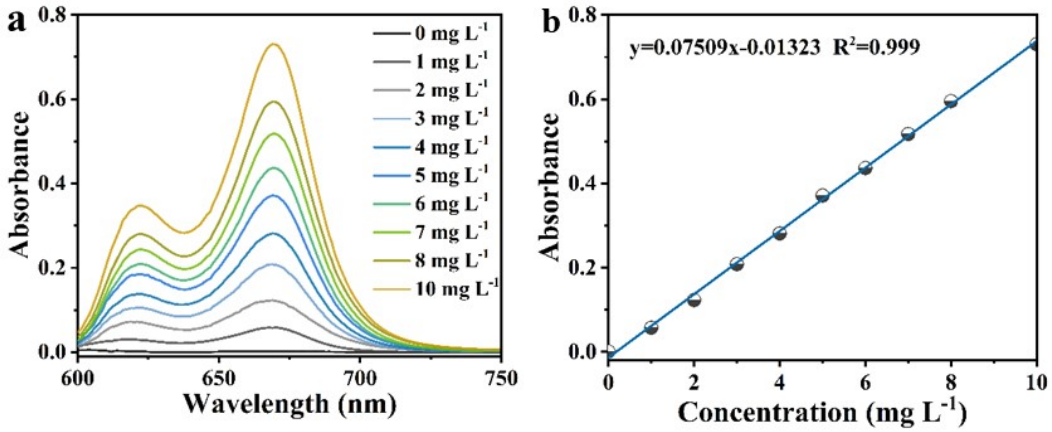

Fig. S10. (a) UV-Vis absorption spectra of various uranyl concentrations after incubation for 20 min at room temperature. (b) Calibration curve used for calculation of uranyl concentrations.

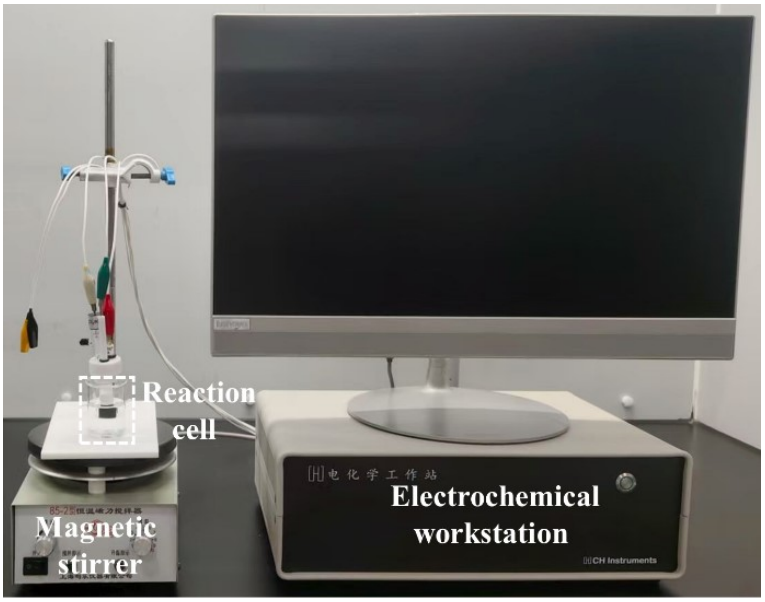

Fig. S11. Reaction device for the batch experiment.

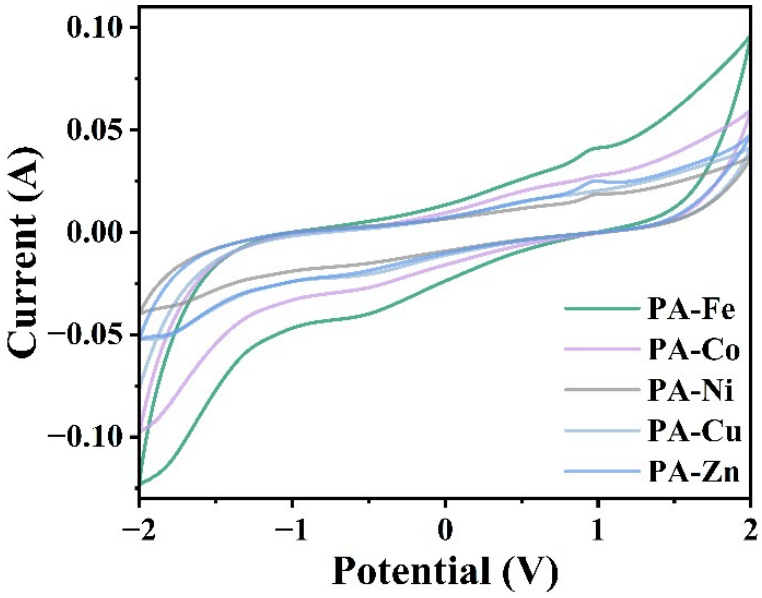

Fig. S12. CV curves of CF@MPN in which PA chelates with different metal ions. The Na_2SO_4 electrolyte contains 5 mg L^{-1} uranyl.

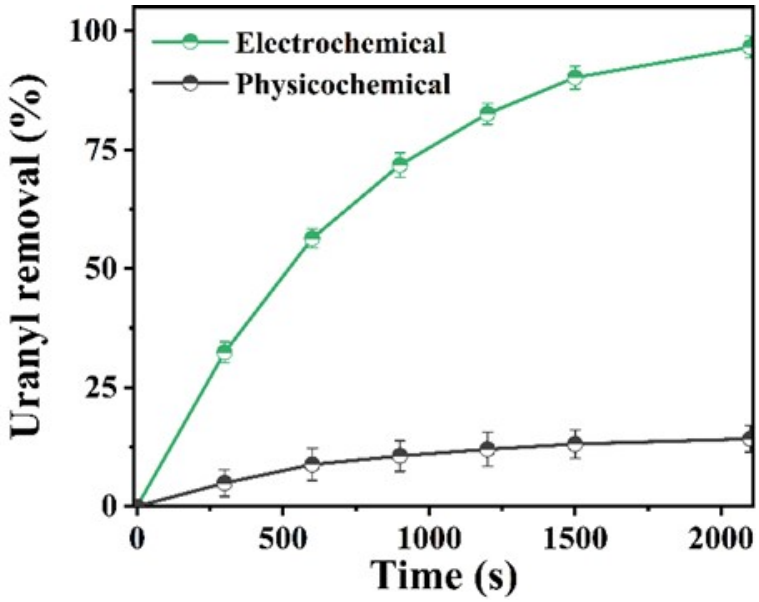

Fig. S13. Comparison of uranyl removal efficiency between physicochemical and electrochemical (−0.5 V) adsorption using CF@MTPN.

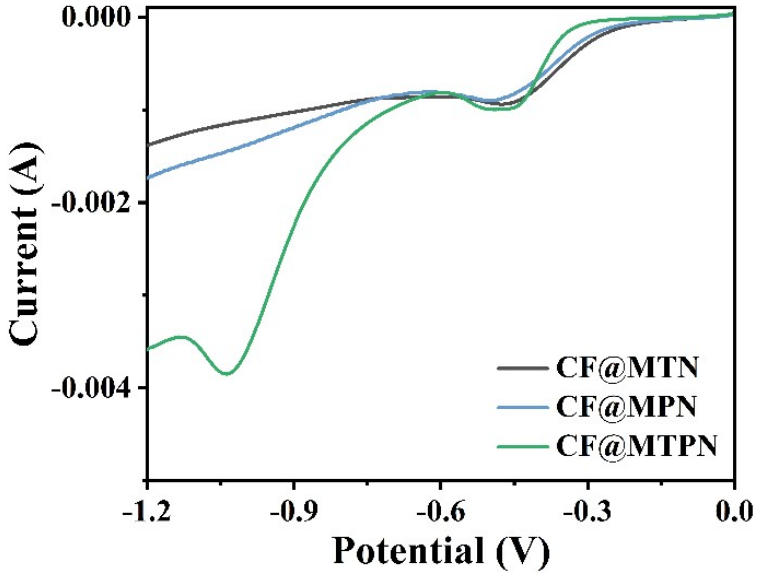

Fig. S14. LSV curves of CF@MTN, CF@MPN and CF@MTPN in 0.1 M Na_2SO_4 electrolyte containing 5 mg L^{-1} uranyl.

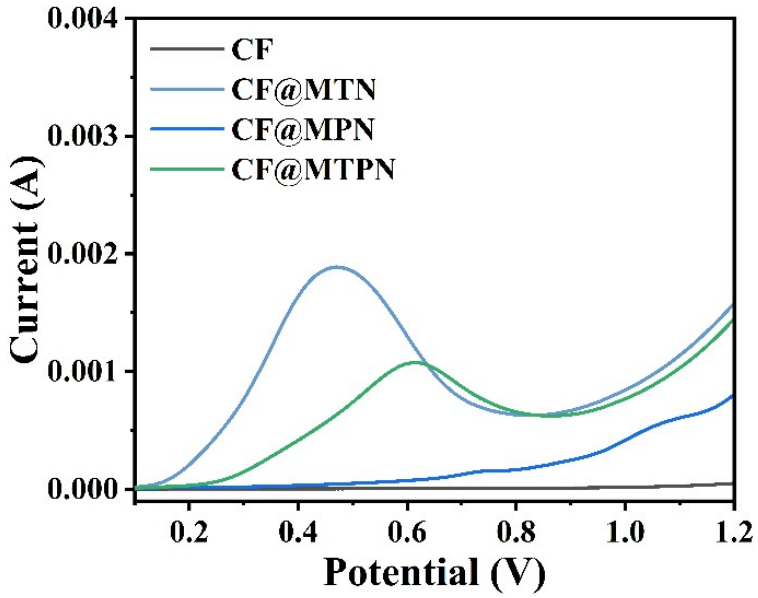

Fig. S15. First round of LSV curves for CF, CF@MTN, CF@MPN and CF@MTPN.

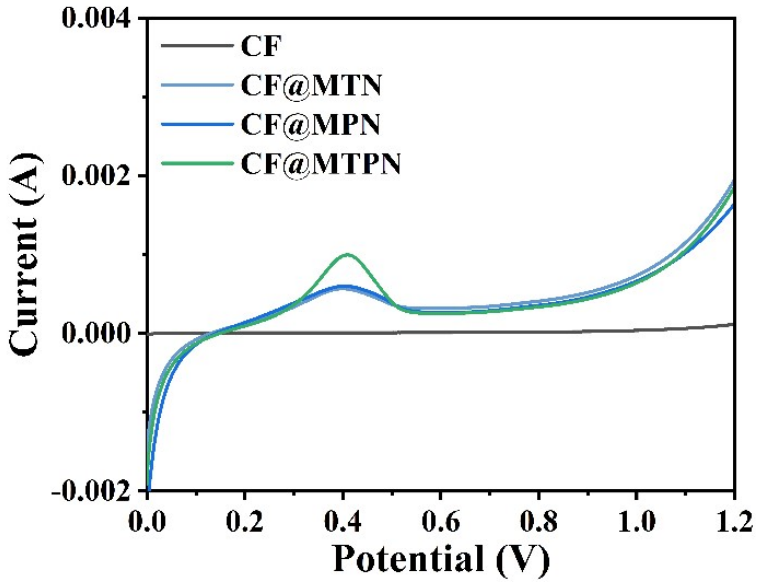

Fig. S16. Tenth round of LSV curves for CF, CF@MTN, CF@MPN and CF@MTPN.

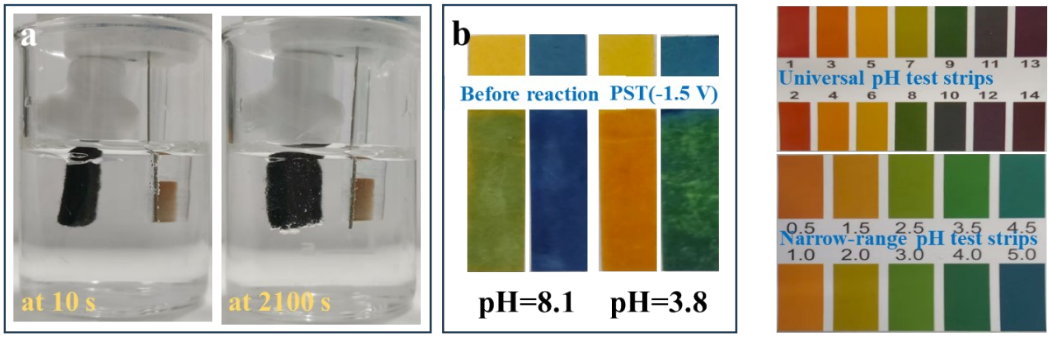

Fig. S17. (a) Digital photos of the electrodes during PST (−1.5 V) at 10 and 2100 s. (b) The pH of the electrolytes before and after the reaction. The values were provided by the pH meter.

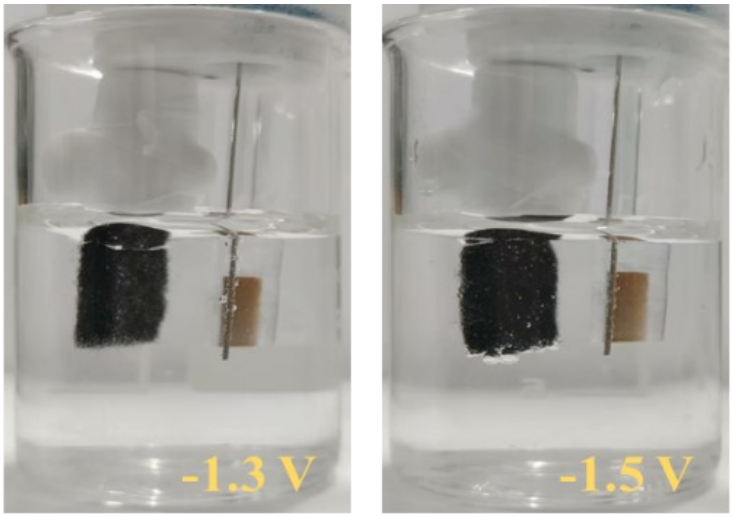

Fig. S18. Digital photos of the CF@MTPN electrode during PST (−1.3 and −1.5 V).

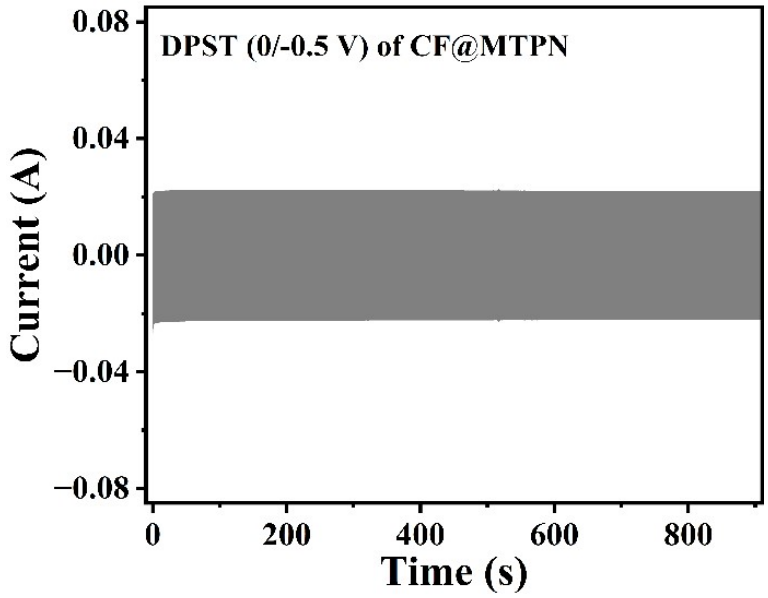

Fig. S19. Chronoamperometric curves of the DPST process (from 0 V to −0.5 V and back to 0 V, periodically) for CF@MTPN. The ratio of power-on time to power-off time is 3:2. The frequency is 400 Hz.

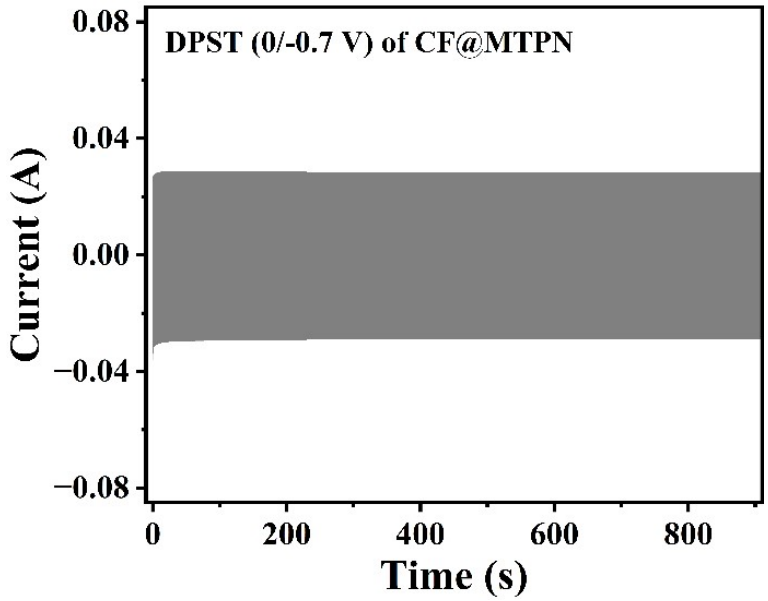

Fig. S20. Chronoamperometric curves of the DPST process (from 0 V to −0.7 V and back to 0 V, periodically) for CF@MTPN. The ratio of power-on time to power-off time is 3:2. The frequency is 400 Hz.

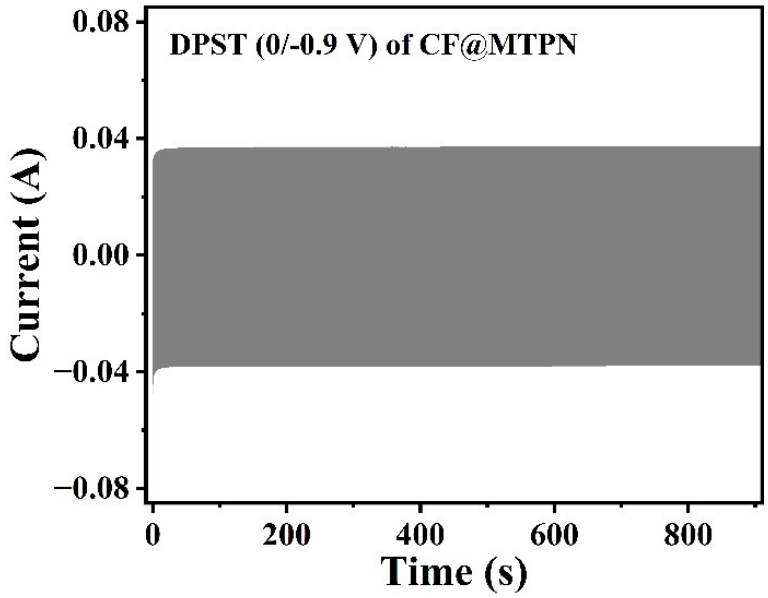

Fig. S21. Chronoamperometric curves of the DPST process (from 0 V to −0.9 V and back to 0 V, periodically) for CF@MTPN. The ratio of power-on time to power-off time is 3:2. The frequency is 400 Hz.

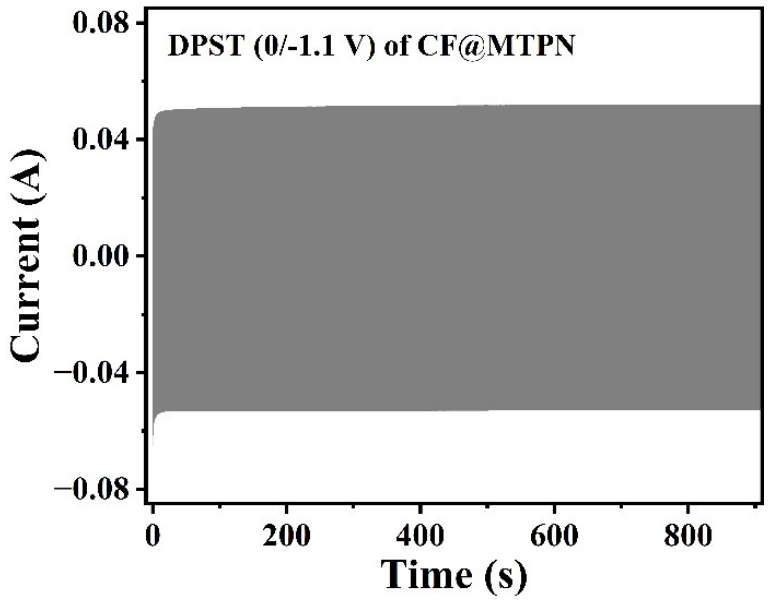

Fig. S22. Chronoamperometric curves of the DPST process (from 0 V to −1.1 V and back to 0 V, periodically) for CF@MTPN. The ratio of power-on time to power-off time is 3:2. The frequency is 400 Hz.

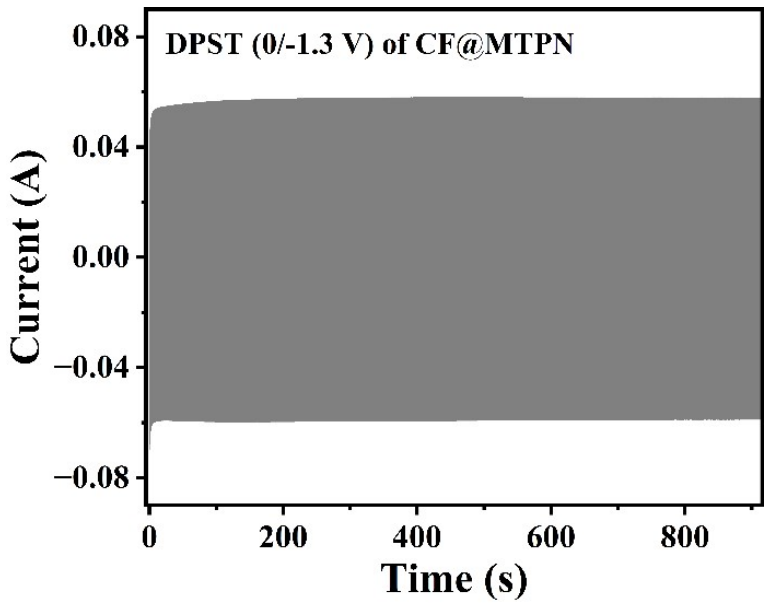

Fig. S23. Chronoamperometric curves of the DPST process (from 0 V to −1.3 V and back to 0 V, periodically) for CF@MTPN. The ratio of power-on time to power-off time is 3:2. The frequency is 400 Hz.

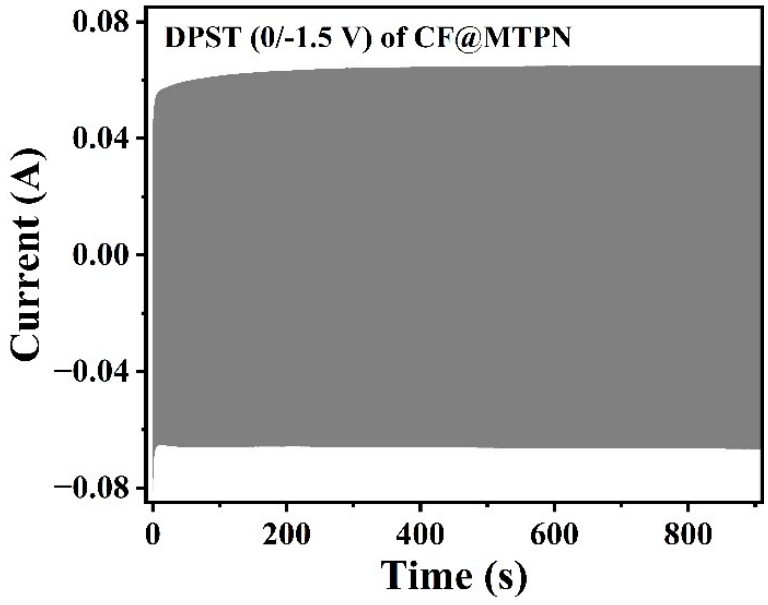

Fig. S24. Chronoamperometric curves of the DPST process (from 0 V to −1.5 V and back to 0 V, periodically) for CF@MTPN. The ratio of power-on time to power-off time is 3:2. The frequency is 400 Hz.

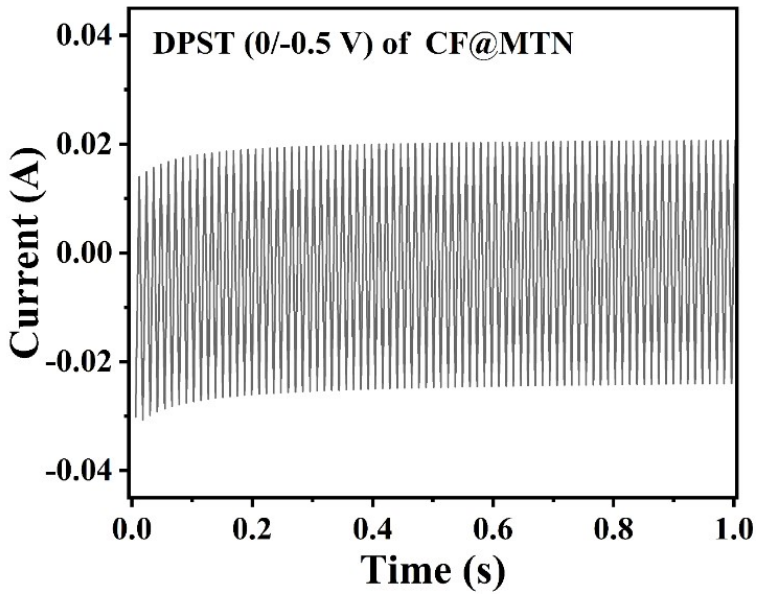

Fig. S25. Pulsed current profile of CF@MTN over the first minute of the DPST process (from 0 V to −0.5 V and back to 0 V, periodically). The ratio of power-on time to power-off time is 3:2. The frequency is 400 Hz.

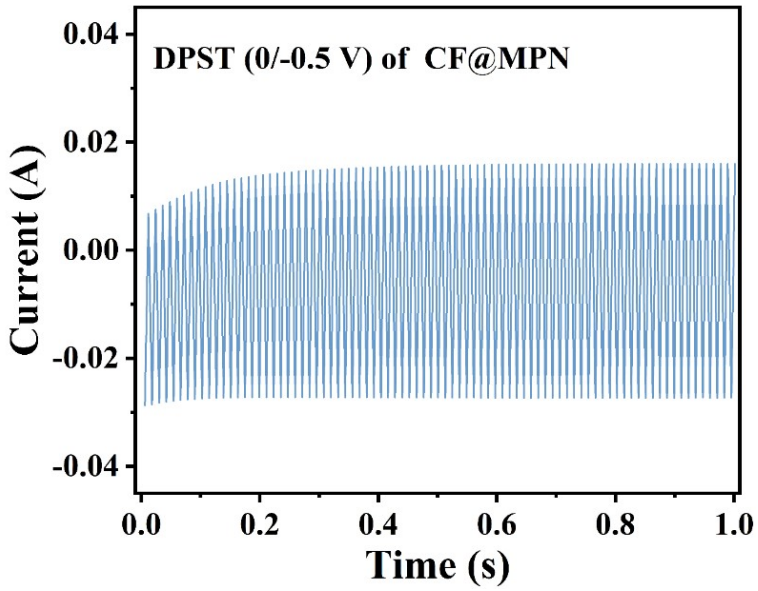

Fig. S26. Pulsed current profile of CF@MPN over the first minute of the DPST process (from 0 V to −0.5 V and back to 0 V, periodically). The ratio of power-on time to power-off time is 3:2. The frequency is 400 Hz.

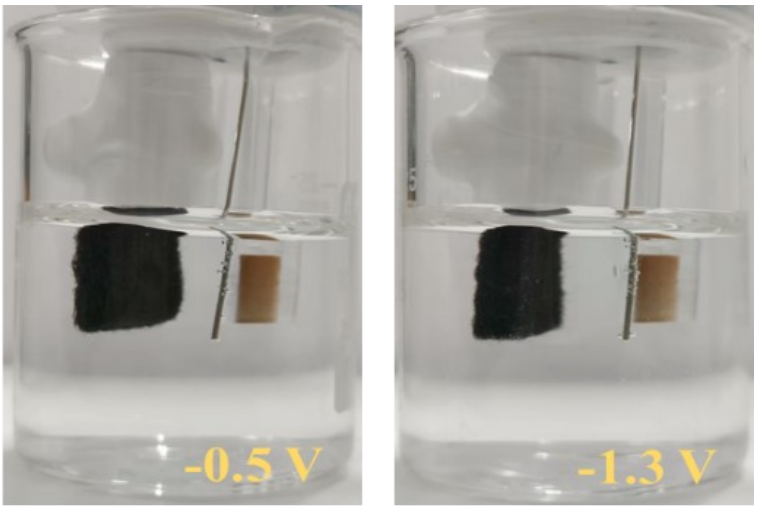

Fig. S27. Digital photos demonstrating the absence of gas bubbles on the CF@MTPN electrode during the DPST process from 0 V to −0.5 V (or −1.3 V) and back to 0 V.

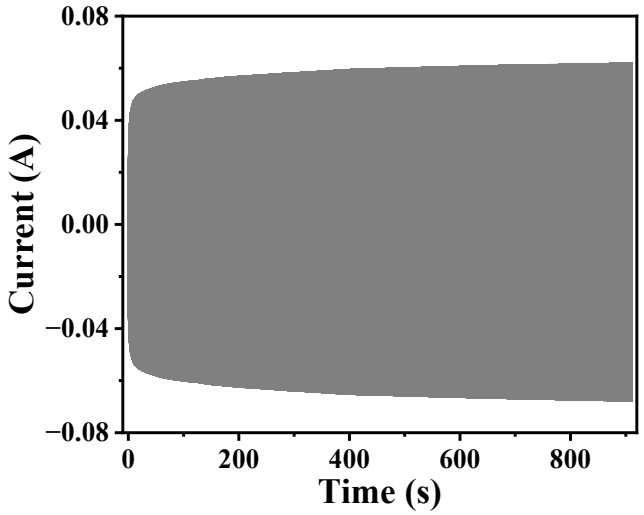

Fig. S28. Chronoamperometric curves of the DPST process (from 0 V to −1.3 V and back to 0 V, periodically) for CF. The ratio of power-on time to power-off time is 3:2. The frequency is 400 Hz.

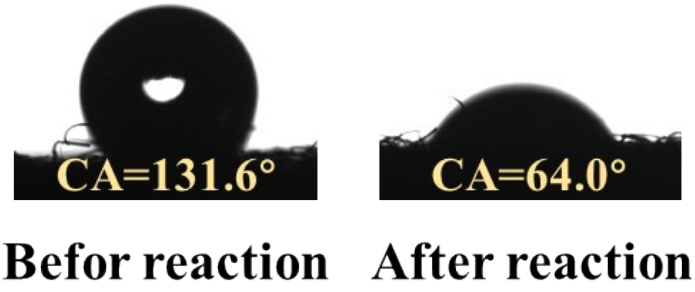

Fig. S29. Water contact angles on CF surfaces before and after use.

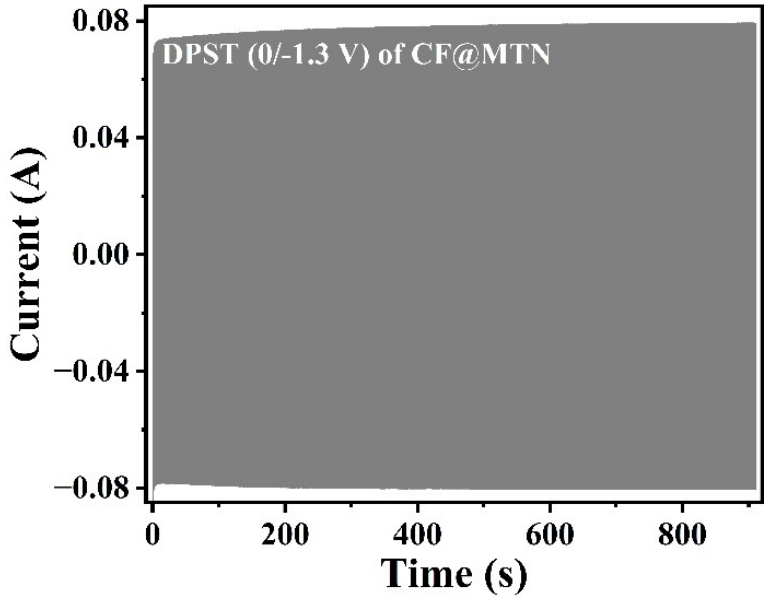

Fig. S30. Chronoamperometric curves of the DPST process (from 0 V to −1.3 V and back to 0 V, periodically) for CF@MTN. The ratio of power-on time to power-off time is 3:2. The frequency is 400 Hz.

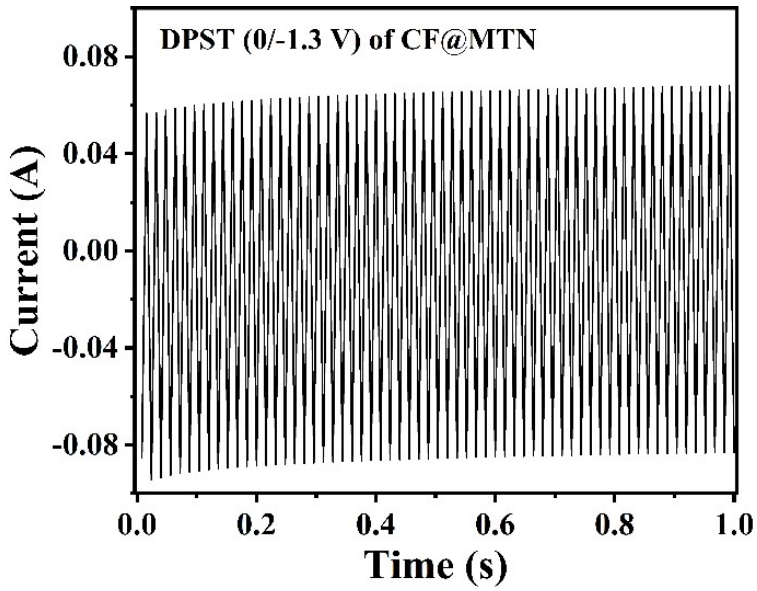

Fig. S31. Pulsed current profile of CF@MTN over the first minute of the DPST process (from 0 V to −1.3 V and back to 0 V, periodically).

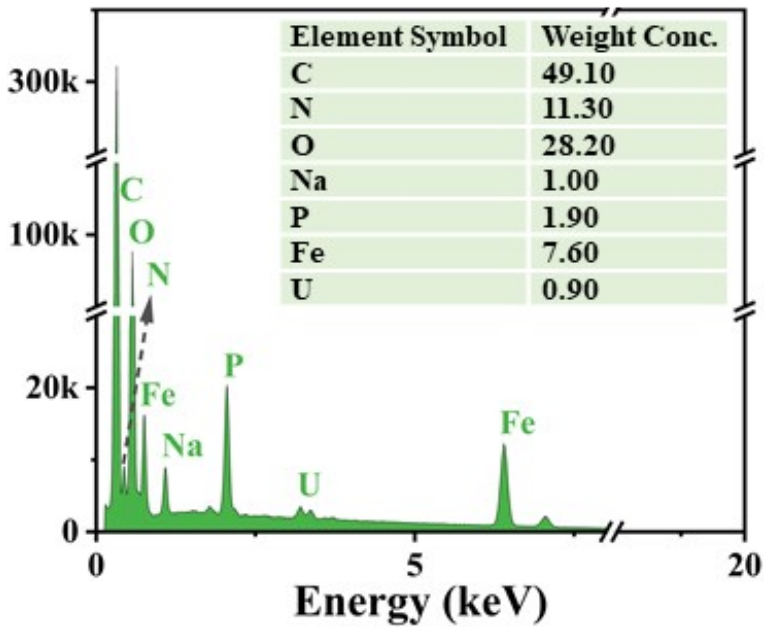

Fig. S32. EDX spectrum of the used CF@MTPN.

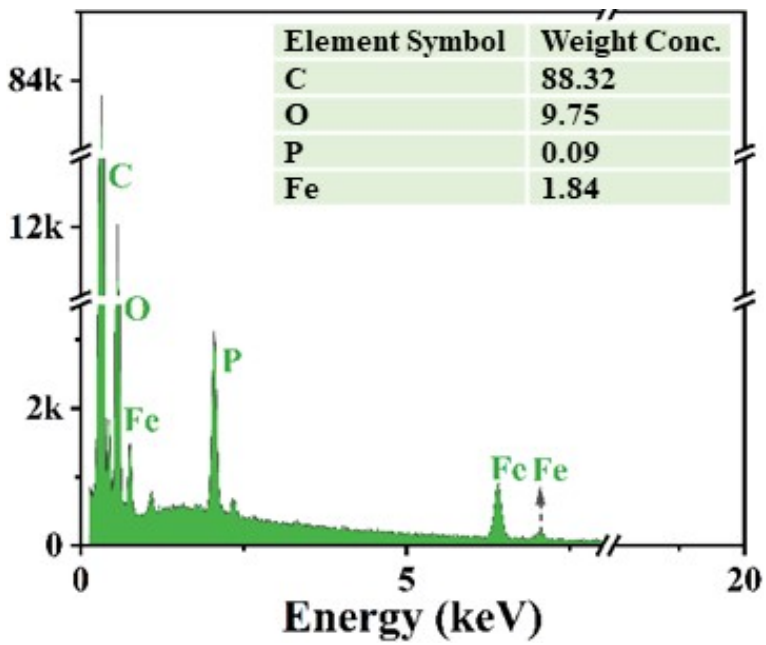

Fig. S33. EDX spectrum of the regenerated CF@MTPN. Uranium was eluted from CF@MTPN by 1.0 M Na_2CO_3 solution.

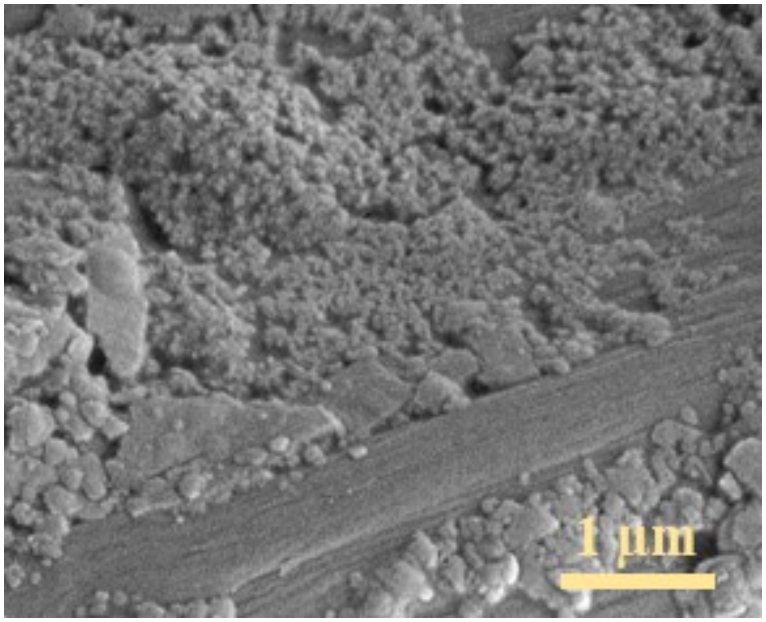

Fig. S34. SEM image of the regenerated CF@MTPN.

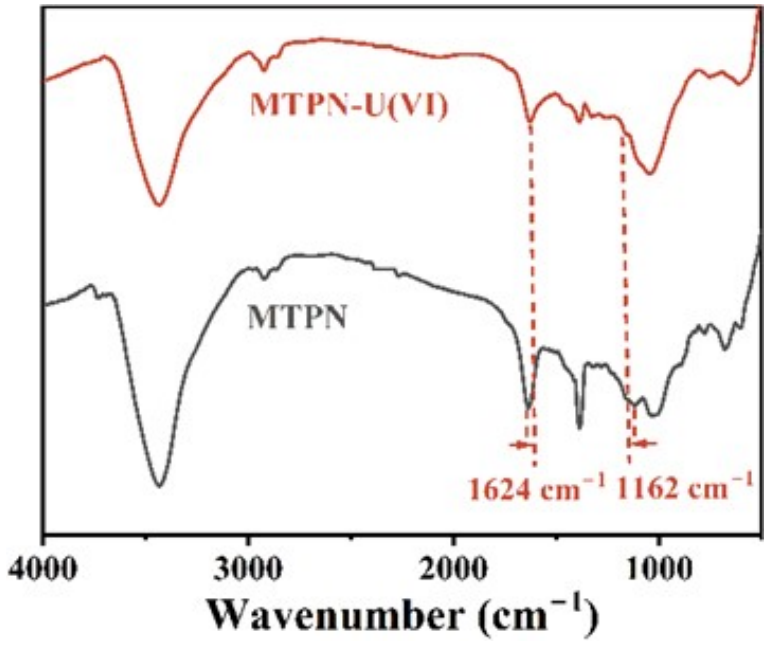

Fig. S35. FTIR spectra of the used and the regenerated CF@MTPN.

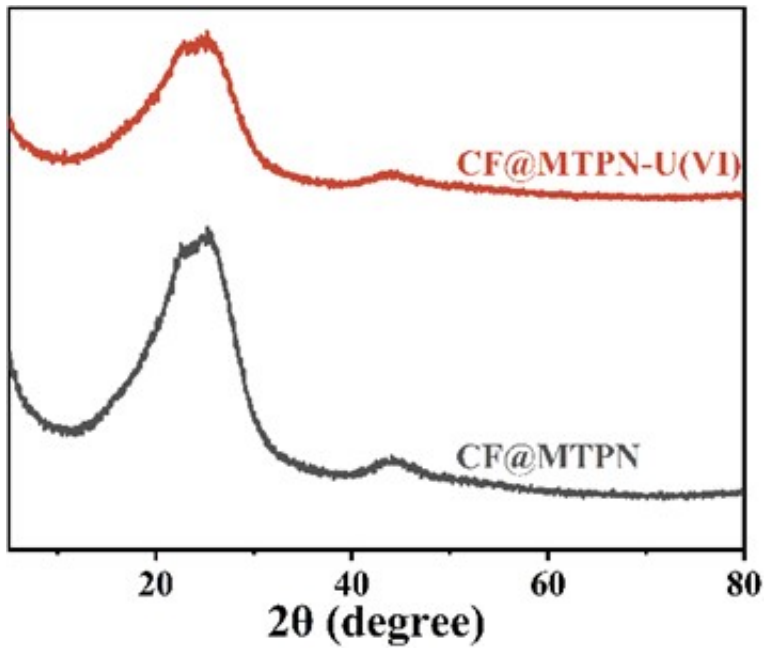

Fig. S36. XRD patterns of the used and the regenerated CF@MTPN.

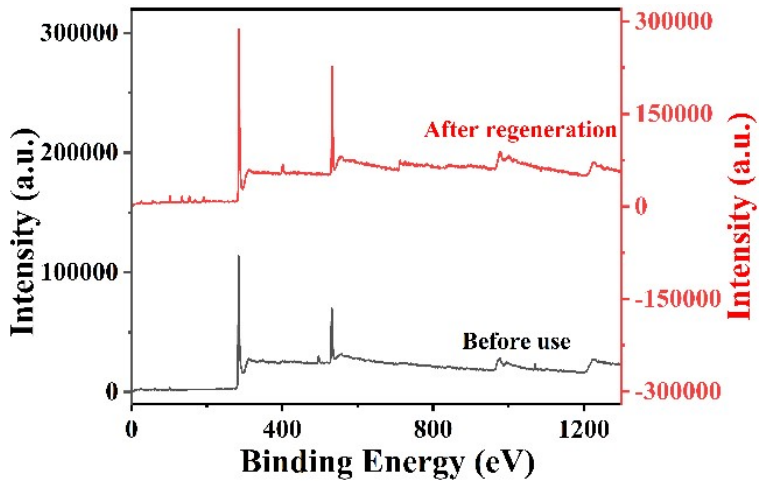

Fig. S37. XPS survey maps of CF@MTPN before use and after regeneration.

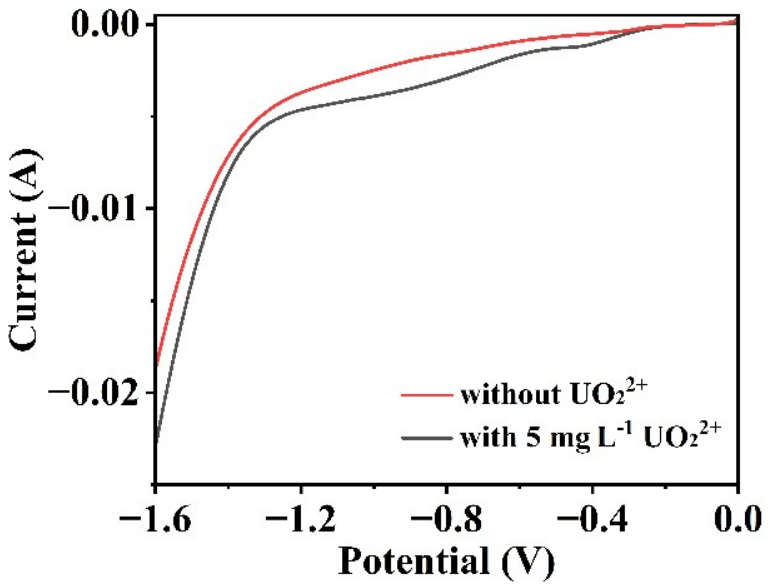

Fig. S38. LSV curves of the regenerated CF@MTPN in 0.1 M Na_2SO_4 with and without 5 mg L^{-1} uranyl.

Table S1 Comparison of the CF@MTPN electrode / adsorbent with the reported materials in the uranium extraction.

Reaction system	Conditions	Process	Electrolytes / Solutions	Extraction capacity	Ref.
Bipolar system (In−N_x−C−R[a]/CF[b] as WE[c], graphite rod as CE[d])	Calculated by weight of In−Nx−C−R	Square wave method (−5 V to 0 V)	Natural seawater	6.35 mg g^{-1} d^{-1}	2
Bipolar system (NZVC[e] as WE, TS[f] as CE)	Calculated by area of NZVC	PST[g] (0.6 V)	East seawater (adjusted to pH 5)	0.009 mg cm^{-2} d^{-1}	3
Three-electrode system (CMOS@NSF[h] as WE)	Calculated by weight of CMOS@NSF	PST (−1.4 V vs. Ag/AgCl)	Natural seawater	2.65 mg g^{-1} d^{-1}	4
Three-electrode system (Mo_2C/MoO_x/CF as WE)	Calculated by weight of Mo_2C/MoO_x	PST (−5 V vs. Ag/AgCl)	Natural seawater (8 ppb uranium)	2.4 mg g^{-1} d^{-1}	5
Bipolar-electrode system (PPA@MISS-PAF-1[i] as WE, graphite rod as CE)	Calculated by weight of PPA@MMIS-PAF-1	AACE[j] (−1.3 V to 0V)	Natural seawater (3.3 ppb uranium)	0.23 mg g^{-1} d^{-1}	6
Three-electrode system ($Ca_5(PO_4)_3(OH)$-Bi_2O_{3-x}/CF as WE)	Calculated by weight of $Ca_5(PO_4)_3(OH)$-Bi_2O_{3-x}	PST (−1.75 V vs. Ag/AgCl)	100 mg/L uranyl, 30 g/L F	0.986 mg g^{-1} d^{-1}	7
Bipolar system (Fe–N_x–C–R[k] as WE, graphite rod as CE)	Calculated by weight of Fe–N_x–C–R	Square wave method (−5 V to 0 V)	Natural seawater (10 ppm uranium)	1.2 mg g^{-1} d^{-1}	8
Three-electrode system (PA-PPy[l]/CF as WE)	Calculated by area of CF	DPST[m] (−5 V to 0 V, vs. SCE)	10 mg/L uranyl nitrate, pH 5	0.17 mg cm^{-2} d^{-1}	9
Bipolar system (PA-PANI/GS[n] as WE, graphite rod as CE)	Calculated by weight of PANI	PST (−1.2 V)	3 ppm uranium	44.33 mg g^{-1} d^{-1}	10
Bipolar system (C-Ami[o] as WE, graphite rod as CE)	Calculated by weight of C-Ami	HW-ACE[p] (−5 V to 0 V)	0.15 ppm uranium	0.16 mg g^{-1} d^{-1}	11
Physicochemical adsorption (PTU[q] as adsorbent)	Calculated by weight of PTU	Adsorption	Natural seawater	0.026 mg g^{-1} d^{-1}	12
physicochemical adsorption (MF@TBAs[r] as adsorbent)	Calculated by weight of MF@TBAs	Adsorption	Natural seawater	2.55 mg g^{-1} d^{-1}	13
Three-electrode system (CF@MTPN as WE)	**Calculated by weight of CF@MTPN**	**DPST (−1.3 V vs. SCE)**	**0.1 M Na_2SO_4, 2 mM Na_2CO_3, 5 ppm uranium**	**99.31 mg g^{-1} d^{-1}**	**This work**
Three-electrode system (CF@MTPN as WE)	**Calculated by CF@MTPN**	**DPST (−1.3 V vs. SCE)**	**Natural seawater**	**3.62 mg g^{-1} d^{-1}**	**This work**

[a] In−N_x−C−R: the functionalized indium−nitrogen−carbon catalyst, where R represents the amidoxime groups;

[b] CF: carbon felt;

[c] WE: working electrode;

[d] CE: counter electrode;

[e] NZVC: nanoscale zero-valent copper;
[f] TS: titanium sheets;
[g] PST: potentiostatic technique;
[h] CMOS@NSF: Ni_3S_2 fiber with polyoxometalate $CoMo_6$-derived amorphous CoMoOS layer;
[i] PPA@MISS-PAF-1: polyphenylacetylacetylene-modified molecularly imprinted porous aromatic framework;
[j] AACE: asymmetrical alternating current electrochemical method;
[k] Fe−N_x−C−R: the functionalized iron–nitrogen–carbon catalyst, where R represents the amidoxime groups;
[l] PA-PPy: phytic acid-doped polypyrrole;
[m] DPST: double potential step technique;
[n] PA-PANI/GS: phytic acid-doped polyaniline / glassy carbon electrode;
[o] C-Ami: amidoxime-functionalized CF electrode;
[p] HW-ACE: half-wave rectified alternating current electrochemical (HW-ACE) method;
[q] PTU: porous poly (tannin-urethane) buoy;
[r] MF@TBAs: melamine foam@TBAs, where TBAs by represents the bio-adsorbents by reacting tannin with paraform-aldehyde.

References

1 K.V. Baskaran, A. Saha and S.S. Ghugre, *J. Radioanal. Nucl. Chem.*, 2023, **332**, 5071–5085.

2 X.L. Liu, Y.H. Xie, M.J. Hao, Z.S. Chen, H. Yang, G.I.N. Waterhouse, S.Q. Ma and X.K. Wang, *Adv. Sci.*, 2022, **9**, 2201735.

3 Y.J. Wang, G.B. Wen, Z.J. Liu, T.T.T. Nga, C.L. Dong, J. You, C. Xie, S.Q. Du, F. Zhang, Q. Liu, J.R. Wei, Y. Cao, X.D. Peng, Y.H. Yuan, Y.Y. Wang and S.Y. Wang, *Nat. Sustainability*, 2025, **8**, 682–691.

4 H.J. Guo, E.M. Hu, Y.H. Wang, Z.H. Ou, B.C. Huang, J. Lei, H.H. Liu, R. He and W.K. Zhu, *Nat. Commun.*, 2025, **16**, 2012.

5 G. Li, J.J. Li, X. Wang, X.C. Deng, H.X. Jin, H. Luo, S.H. Xiao, L.M. Fang, W.K. Zhu and R. He, *Sep. Purif. Technol.*, 2025, **364**, 132496.

6 Z.Y. Wang, Q.H. Meng, R.C. Ma, Z.K. Wang, Y.J. Yang, H.Y. Sha, X.J. Ma, X.H. Ruan, X.Q. Zou, Y. Yuan and G.S. Zhu, *Chem*, 2020, **6**, 1683–1691.

7 G. Li, Y. Liu, C. Jiao, Z.Y. Jiang, J. Zhang, T. Chen, T. Lin, R. He, W.K. Zhu and X.K. Wang, *Water Res.*, 2025, **279**, 123467.

8 H. Yang, X.L. Liu, M.J. Hao, Y.H. Xie, X.K. Wang, H. Tian, G.I.N. Waterhouse, P.E. Kruger, S.G. Telfer and S.Q. Ma, *Adv. Mater.*, 2021, **33**, 2106621.

9 J. Huang, Z.R. Liu, D.J. Huang, T.X. Jin and Y. Qian, *J. Hazard. Mater.*, 2022, **433**, 128775.

10 M.N. Huang, L.S. Xie, Y.J. Wang, H.J. He, H.B. Yu, J.S. Cui, X.G. Feng, Z.N. Lou and Y. Xiong, *Chem. Eng. J.*, 2023, **457**, 141221.

11 C. Liu, P.C. Hsu, J. Xie, J. Zhao, T. Wu, H.T. Wang, W. Liu, J.S. Zhang, S. Chu and Y. Cui, *Nat. Energy*, 2017, **2**, 17007.

12 P. Liu, M.Y. Xu, W.W. Wang, Y. Song, F.J. Wang, X.Y. Peng, L.J. Zhang, S.S. Chen and D.B. Hua, *Sep. Purif. Technol.*, 2025, **362**, 131681.

13 X.Y. Fu, M.S. Shi, D.Y. Chen, Z.X. Ren, Q. Bai and R. Zhao, *Desalination*, 2025, **601**, 118553.